General Search Results--Full Record

Article 9 of 12 SUMMARY RELATED RECORDS

SUBSYNOPTIC-SCALE BAROCLINIC INSTABILITY

SATYAMURTY P, RAO VB, **MOURA AD**

JOURNAL OF THE ATMOSPHERIC SCIENCES
39: (5) 1052-1061 1982

Document type: Article | **Language:** English | **Cited References:** 34 | **Times Cited:** 12

Addresses:
SATYAMURTY P, CONSELHO NACL DESENVOLVIMENTO CIENT & TECNOL, INST PESQUISAS ESPACIAIS, BR-12200 SAO JOSE DOS CAM, SP, BRAZIL.

Publisher:
AMER METEOROLOGICAL SOC, BOSTON

IDS Number:
NV421

ISSN:
0022-4928

Article 9 of 12 SUMMARY

Subsynoptic-Scale Baroclinic Instability

PRAKKI SATYAMURTY, VADLAMUDI BRAHMANANDA RAO AND ANTONIO DIVINO MOURA

Conselho Nacional de Desenvolvimento Científico e Tecnológico—CNPq, Instituto de Pesquisas Espaciais—INPE, São José dos Campos, SP, Brasil

(Manuscript received 30 September 1981, in final form 14 January 1982)

ABSTRACT

A linear stability analysis of the hyperbolic tangent profiles is made. A Boussinesq primitive equation model with high vertical resolution is used. Unstable modes of intermediate scales ($L_x \approx 1000$ km) are generated when the curvature, $d^2\bar{u}/dz^2$, of the basic flow in the lower levels is negative. Even if the curvature in the lower levels is positive, intermediate-scale unstable modes appear for smaller static stability and shear (Richardson number not necessarily small) or for certain vertical distributions of diabatic heating due to the liberation of latent heat in the lower troposphere. The amplitude of the most unstable intermediate-scale wave is confined to the lower troposphere and its growth rate increases with the inclusion of diabatic heating.

1. Introduction

Following the pioneering works of Charney (1947), Eady (1949), Kuo (1952) and Phillips (1954), baroclinic instability as the principal mechanism for the development of atmospheric disturbances received a great deal of attention. Most of the characteristics of middle- and high-latitude disturbances, such as the horizontal scale (L), westward tilt in the vertical and eastward movement of the upper tropospheric synoptic-scale ($L \approx 4000$ km) transient waves are successfully explained by this instability, even within the framework of quasi-geostrophic (QG) theory. However, linear analysis is incapable of completely explaining the concentration of isotherms into frontal zones.

With the ever-increasing density of observations and the advent of satellite-based cloud pictures, transient disturbances of subsynoptic scales ($L < 2000$ km) have been observed in certain preferred locations such as the polar frontal region (Reed, 1979) and along the "Baiu" frontal zone (Matsumoto *et al.*, 1970) in the Northern Hemisphere. Similar disturbances have also been observed, by the authors, to develop or intensify over and around extratropical South America. Carleton (1979) has given observational evidence for local winter cyclogenesis over South America. Some of these disturbances seem to be similar to the frontal waves observed by Bjerknes and studied by Solberg (1928), Eliasen (1960) and Orlanski (1968).

[illegible] whether the upper-air synoptic [illegible] existing frontal zones are [illegible] fronts de[illegible] due to the deformation fields associated [illegible] existing waves is rather controversial (Phillips, 1970). Whatever may be the case, there is a general consensus that the waves and fronts are closely associated. However, it appears that there is a fundamental difference between long upper waves ($L \approx 4000$ km) and the surface frontal waves ($L \approx 1500$ km) which are due to the secondary instabilities of the frontal zone (Charney, 1975).

Most of the earlier linear studies of the baroclinic instability used the QG assumption (i.e., Rossby number, $\mathrm{Ro} \equiv k\bar{u}/f \ll 1$ where k is the zonal wave number, $\bar{u}$ the basic zonal wind and f the Coriolis parameter), while a few used a two-level model of the atmosphere or deliberately took the basic state to have constant vertical shear ($d\bar{u}/dz$) and static stability (S). Kuo (1953) studied quasi-geostrophic baroclinic instability for basic states with constant shear and static stability. His results showed a single maximum in the growth rate curves. He concluded that the amplitude of large-scale waves ($L > 5000$ km) increased with height while that of the shorter waves ($L < 4000$ km) has its maximum at lower levels. Therefore, it is reasonable to believe that the atmospheric conditions in the lower troposphere are more important for the growth and characteristics of the subsynoptic-scale unstable waves.

Stone (1966, 1970) extended the solutions of the Eady model to ageostrophic perturbations. He concluded that the largest growth rates were associated with geostrophic baroclinic instability if Ri [Richardson number $\equiv S/(d\bar{u}/dz)^2$] > 0.95; with symmetric instability if $0.25 < \mathrm{Ri} < 0.95$ and with Kelvin-Helmholtz instability if $0 < \mathrm{Ri} < 0.25$. Staley [illegible] obtained numerically growth rates of baroclinically unstable waves in a four-level QG model. Their results showed the importance of the

0022-49[illegible]/82/051052-10$06.50

vertical variation of the basic state, especially the shear and static stability in the lower levels, for unstable subsynoptic-scale waves. The study of Blumen (1979) with a two-layer QG model demonstrated how the short- and long-wave baroclinic instabilities depended on the relative layer depths as well as on the jump in static stability between the two layers. Extending the study of Blumen, Hyun (1981) found that the shorter-scale instability characteristics were affected also by the jump in shear.

None of the studies mentioned above have examined the baroclinic instability of subsynoptic scales when the basic state's vertical shear and statification simultaneously vary with height. In the present study, we shall examine subsynoptic baroclinic instability with a primitive equation model possessing high vertical resolution.

2. Mathematical formulation

a. Model equations

We consider the inviscid primitive Boussinesq equations (see Duffy, 1978), including diabatic heating. Our basic state (denoted by an overbar) which is independent of time and zonal coordinate, is then perturbed by an infinitesimal wave perturbation propagating in the zonal direction (denoted by a caret). For example, the zonal component of the wind is expressed as

$$u(x, y, z, t) = \bar{u}(y, z) + \mathrm{Re}[\hat{u}(y, z)\exp ik(x - ct)]. \quad (1)$$

The equations governing the perturbations are then found to be

$$\left(k^2\delta - \frac{\partial F}{\partial y} - \delta\frac{\partial^2}{\partial y}\right)\hat{v} + \left(\frac{\partial^2\bar{u}}{\partial y\partial z} + \frac{\partial\bar{u}}{\partial z}\frac{\partial}{\partial y} + F\frac{\partial}{\partial z} - \delta\frac{\partial^2}{\partial y\partial z}\right)\hat{w} = 0, \quad (2)$$

$$\left(\delta F\frac{\partial}{\partial z} + \delta\frac{\partial\bar{u}}{\partial z}\frac{\partial}{\partial y} + \delta^2\frac{\partial^2}{\partial y\partial z} - f\frac{\partial\bar{u}}{\partial z} - \delta\frac{\partial^2\bar{u}}{\partial y\partial z}\right)\hat{v} + \left(S - \delta\frac{\partial^2\bar{u}}{\partial z^2} + \delta^2\frac{\partial^2}{\partial z^2}\right)\hat{w} = \frac{g}{c_p\bar{T}}\hat{H}, \quad (3)$$

where

$$\delta \equiv (\bar{u} - c), \quad F \equiv \left(f - \frac{\partial\bar{u}}{\partial y}\right), \quad S \equiv \frac{g}{\theta_0}\frac{\partial\bar{\theta}}{\partial z}, \quad (4)$$

and where c is the complex phase speed, θ_0 a constant reference potential temperature, H the rate of diabatic heating and the remaining symbols have the usual meaning. Besides considering the atmosphere to be hydrostatic, other approximations used to arrive at (2) and (3) are that $\theta_0 \gg \bar{\theta}$ or $\hat{\theta}$, implied in the Boussinesq approximation, and the linearization.

Eqs. (2) and (3) are two simultaneous partial differential equations in $\hat{v}$ and $\hat{w}$ which may be solved once the basic state and the heating functions are specified. On the other hand, if the heating is taken to be zero or is only a function of the dependent variables, the equations become homogeneous and an eigenvalue problem occurs, in which c is the eigenvalue and $\hat{v}$ and $\hat{w}$ constitute the eigenfunction. In any case, analytical solutions are difficult to obtain. Numerical solutions may however be obtained using a finite difference grid in the y–z plane. The problem reduces to finding eigenvalues and eigenvectors of a very large complex matrix, for a reasonable resolution in both y and z directions. Therefore the problem has been further simplified.

Under the mean conditions, the meridional shear of the zonal wind ($\partial\bar{u}/\partial y$) is of the order of 10^{-5} s^{-1}, whereas the Coriolis parameter is taken to be of the order of 10^{-4} s^{-1}. Thus F may be approximated by f and, by the same argument, $(\partial^2\bar{u}/\partial y\partial z)\hat{w}$ may be neglected in comparison with $f(\partial\hat{w}/\partial z)$ in (2) and $\delta(\partial^2\bar{u}/\partial y\partial z)$ may be neglected in comparison with $f(\partial\bar{u}/\partial z)$ in (3). Therefore a justifiable simplification would be to consider the basic state zonal wind to be independent of y. This approximation does not hold in strong frontal zones. However, for simplifying the problem the above approximation is used. Considering $df/dy = \beta$ to be constant (β-plane approximation), the coefficients of (2) and (3) become independent of y and will allow us to assume the structure of the dependent variables to be sinusoidal in y; $\hat{w} = \tilde{w}\exp(ily)$. This kind of structure is in fact necessary for the separability of Eqs. (2) and (3). Introducing these simplifications into (2) and (3) and eliminating $\hat{v}$, we arrive at a single equation for $\tilde{w}$:

$$A\frac{d^2\tilde{w}}{dz^2} + B\frac{d\tilde{w}}{dz} + C\tilde{w} = Q, \quad (5)$$

where

$$\begin{aligned} A &= D\delta(f^2 + l^2\delta^2 + D\delta) \\ B &= \frac{d\bar{u}}{dz}[\delta(k^2 + l^2)(f^2 + l^2\delta^2) - D(f - il\delta)^2] \\ C &= \left(\frac{d\bar{u}}{dz}\right)^2[il\delta(k^2 + l^2)(f + il\delta) - ilD(f - il\delta)] \\ &\quad + [il\delta D(f + il\delta)]\frac{d^2\bar{u}}{dz^2} + D^2\left(S - \delta\frac{d^2\bar{u}}{dz^2}\right) \\ Q &= \frac{D^2g}{c_p\bar{T}}\hat{H}, \quad D \equiv [\beta - (k^2 + l^2)\delta] \end{aligned} \quad (6)$$

The only form of diabatic heating employed in this study is that due to the liberation of latent heat, for which the wave-CISK (Chang, 1976) mechanism is assumed. Consequently we write the heating term

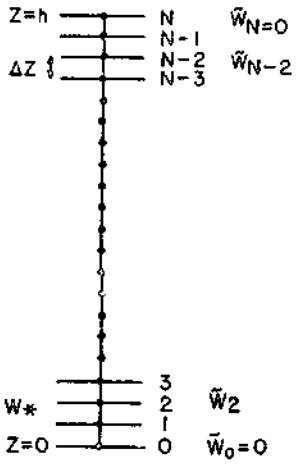

FIG. 1. Vertical Grid.

as

$$Q = D^2 S(z)\eta(z)\tilde{w}_* , \qquad (7)$$

where $\tilde{w}_*$ is the vertical velocity at the cloud base level and $\eta(z)$ is a non-dimensional vertical distribution function. This kind of parameterization is mathematically convenient for posing an eigenvalue problem. CISK is a mechanism more appropriate for the tropical atmosphere but there have been instances in which it is invoked to explain extratropical phenomena (Nitta, 1964; Rasmussen, 1979). For secondary instabilities on pre-existing frontal zones, liberation of latent heat from convective clouds is important (Nitta and Ogura, 1972). Eq. (5) becomes homogeneous once (7) is introduced into (6).

b. *Method of solution*

Eq. (5) with the coefficients given by (6) and (7) is applied at the intermediate levels of the grid shown in Fig. 1. If centered finite-differences are used, (5) becomes

$$A'_n\tilde{w}_{n+1} + B'_n\tilde{w}_n + C'_n\tilde{w}_{n-1} + D'_n\tilde{w}_m = 0,$$
$$n = 1, 2, 3, \cdots N-1, \qquad (8)$$

where N is the maximum number of layers of depth Δz into which the atmosphere is divided, m represents cloud base level,

$$\left.\begin{aligned} A_n &= \left(\frac{A}{\Delta z^2} + \frac{B}{2\Delta z}\right)_n ; \quad B'_n = \left(C - \frac{2A}{\Delta z^2}\right)_n \\ C'_n &= \left(\frac{A}{\Delta z^2} - \frac{B}{2\Delta z}\right)_n ; \quad D'_n = (k^2\eta S[c - \bar{u}])_n \end{aligned}\right\}, \qquad (9)$$

... value at the level n. The

$$\tilde{w}_0 = \tilde{w}_N = 0. \qquad (10)$$

The system of equations (8) forms a linear algebraic homogeneous set which can be written as

$$(c^4\mathbf{P} + c^3\mathbf{Q} + c^2\mathbf{R} + c\mathbf{S} + \mathbf{T})\mathbf{W} = 0, \qquad (11)$$

where **P**, **Q**, **R**, **S** and **T** are complex square matrices of order $(N-1) \times (N-1)$ whose elements are functions of the basic state variables and **W** is the column vector formed by $\tilde{w}_1, \tilde{w}_2, \cdots \tilde{w}_{N-1}$. We note that (11) constitutes a generalized eigenproblem. Solving it amounts to obtaining ... genvectors of a complex matrix of the order $(4N-4) \times (4N-4)$. The problem can be solved by using the algorithms developed by Garbow (1978).

For a given basic state [$\bar{u}(z)$, $S(z)$, f and β] and zonal wavelength $L_x = 2\Pi/k$, the eigenvalues $c = c_r + ic_i$, and the eigenvectors $\mathbf{W} = W_r + iW_i$ are obtained. The procedure is repeated for several values of L_x between 100 and 10 000 km to obtain e-folding times $(1/kc_i)$. The graph of the e-folding times versus L_x will hereafter be referred to as IS (instability spectrum).

Having obtained $\tilde{w}$ for the modes with maximum instability (or minimum e-folding time) $\tilde{v}$ is obtained from the simplified version of (2), $\tilde{u}$ is obtained by using continuity equation, geopotential $\tilde{\phi}$, the x-component equation of motion and $\tilde{\theta}$ the hydrostatic approximation.

c. *Basic state*

The procedure outlined above can be used to obtain the IS of any zonal wind and static stability profiles. We are interested in examining the instability characteristics of the intermediate scale ($L \approx 1500$ km) disturbances in the vicinity of baroclinic zones associated with idealized weak thermal fronts. Thus the profiles considered are mathematically expressed as

$$\left.\begin{aligned} \bar{u} &= -\frac{a}{2f\gamma}\left[\tanh\left(\frac{y_0 + \gamma z}{d}\right) - \tanh(y_0/d)\right] \\ \bar{\theta} &= \frac{a\theta_0}{2g}\left[\tanh\left(\frac{y_0 + \gamma z}{d}\right)\right] \end{aligned}\right\}, \qquad (12)$$

where y_0 is the meridional distance of the center of the surface frontal zone from the vertical section where the profiles are taken; $d, 1/\gamma$ and a are the half width, slope and the intensity of the frontal zone, respectively. If we vary both z and y_0, (12) produces a meridional section of the mean zonal conditions in an idealized frontal zone. The point $z = 0$ and $y_0 = 0$ corresponds to the midpoint of the frontal zone at the bottom boundary. The governing equation (5) is independent of ... and therefore the vertical profiles ... at any location across the frontal zone may be obtained by choosing y_0 properly.

The profiles of $\bar{u}$ and $\bar{\theta}$ obtained by (12) for dif-

TABLE. Idealized theoretical profiles and their ... (see Eq. (12)).*

Symbol	Latitude (°S)	y_0 (km)	Ri_m	$(S_m; S_a)$ (10^{-4} s^{-2})	$(d\bar{u}/dz)$ (10^{-3} s^{-1})	(h_c) (km)
P1	30	−800	4.7	1.5; 0.8	5.7	3
**P1L	30	−800	8.2	0.8	3.1	—
P2	30	0	3.2	1.5; 0.5	6.8	0
**P2L	30	0	4.0	0.2	2.3	—
P3	45	+800	8.2	0.8; 0.2	3.2	0

* Latitude = latitude of intersection of the frontal zone with the surface ($z = 0$)
y_0 = meridional distance of the vertical cross section at which the profile is obtained from the surface frontal zone
Ri_m = minimum value of the Richardson number
$(S_m; S_a)$ = maximum and average values of the static stability
$(d\bar{u}/dz)$ = maximum value of the vertical shear
(h_c) = height below which $d^2\bar{u}/dz^2 > 0$; level at which (S_m); $(d\bar{u}/dz)$ and Ri_m occur.

** Profiles P1L and P2L are obtained from P1 and P2, respectively, by joining the extremes by straight lines (see Fig. 2). In these profiles S, $d\bar{u}/dz$ and Ri are constants.

ferent values of y_0 and f and for carefully chosen values of a, d, γ and θ_0 are shown in Fig. 2 (see also Table 1). The basic state obtained for the values of $\theta_0 = 295$ K, $a = 1$ m s^{-2}, $\gamma = 300$, $d = 1000$ km and f at 45°N agreed very well with those observed by Mullen (1979) in situations in which comma-type disturbances developed (see Fig. 2 of Mullen, 1979).

In the inviscid QG fluid the necessary condition for the presence of dynamic instability is the existence of either a meridional thermal gradient at the surface or a change in the sign of $\partial\bar{q}/\partial y$ (where $\bar{q}$ is a pseudo potential vorticity) somewhere in the domain (Charney, 1973). In the profiles given by (12), $\partial^2\bar{q}/\partial y\partial z$ is zero if β is taken to be a constant and, therefore, the quasi-geostrophic IS of these profiles would present only the Eady or Charney modes. Any additional modes can be attributed to ageo...

d. Comments on the governing equation

The present model takes into account the effects of the curvature of the basic zonal wind profiles and the ageostrophic terms. In the usual QG formulation the terms $k^2\delta^2$ and $l^2\delta^2$ are neglected in comparison with f^2 in the coefficients given in (6). For the intermediate-scale disturbances (L_x, $L_y \approx 1500$ km) this approximation is not justified. The retention of these terms may generate additional modes of instability relevant to subsynoptic scale waves and/or modify the existing instability characteristics. When constant shear profiles of $\bar{u}$ are considered the second term and a part of the third term of C in (6) drop out. The vertical shear variation ($d^2\bar{u}/dz^2$), hereafter referred to as curvature, may have a destabilizing effect on the zonal flow. The third term of C shows clearly that under certain favorable conditions the effective value of the static stability may be less by 20–30%, at least in some layers of the atmosphere (typical values are: $S \approx 10^{-5}$ s^{-1}, $d^2\bar{u}/dz^2 \approx 10$ m^{-1} s^{-1} and $\delta \sim 10$ m s^{-1}). In addition, this term changes the character of the governing equation because C will have a term in c^3 in this case, even if $l = 0$. Since the effect of the reduction of the static stability is felt more by the subsynoptic-scale waves, the curvature effect turns out to be more important for these waves. If β, $d^2\bar{u}/dz^2$ and Q are taken to be zero in (5), our perturbation equation reduces to Eq. (1.2) in Stone's (1966) paper.

3. Discussion of the results

Table 2 describes those cases discussed in this section. In all cases the total atmospheric depth (h) is taken to be 10 km, which is divided into 20 layers of 0.5 km thickness. However, tests with several grid resolutions (Δz) between 0.4 and 2.0 km were made

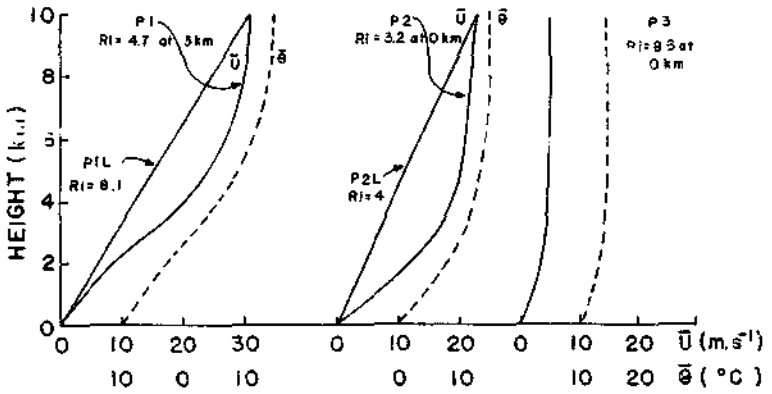

FIG. 2. Vertical profiles of the basic zonal wind ($\bar{u}$) and potential temperature ($\bar{\theta}$) (see also Table 1).

TABLE 2. Cases in which the instability spectra (IS) are obtained.

Case number	Profile used	Special characteristics	Figure number
1	P1L	Repetition of the Eady mode	3
2	P1	Effect of $d^2\bar{u}/dz^2 > 0$ in the lower levels on the IS	3
3	P2L	Eady mode with smaller S	4, 5
4	P2	$d^2\bar{u}/dz^2 > 0$ throughout	4, 5
5	P3	Small S and $d^2\bar{u}/dz^2 < 0$ throughout	6
6	P1	Reduced fluid depth	3
7	P1	$\eta = \eta_1$, heating maximum in the upper troposphere	8
8	P1	$\eta = \eta_2$, heating maximum in the middle troposphere	8
9	P1	$\eta = \eta_3$, heating maximum in the lower troposphere	8
10	P2	$\eta = \eta_4$, same as case 4 but with upper tropospheric heating	10
11	P3	$\eta = \eta_4$, same as case 5 except with upper tropospheric heating	6, 11
12	P1L	$\beta \neq 0$, Eady-Charney mode	12
13	P1	$\beta \neq 0$, Eady-Charney mode modified by curvature	12
14	P1	As in case 13 except η_4 included	12
15	P1	As in case 13 except $l = k$	12
16	P2	As in case 10 except $\beta \neq 0$	10

and the resolution of $\Delta z = 0.5$ km was found to be quite adequate. For wavelengths less than 2000 km, inaccurate results were obtained with $\Delta z > 1.0$ km.

a. *Results with $\beta = 0$, $l = 0$*

The growth rates for cases 1 and 2 are shown in Fig. 3. The region of instability found at wavelengths

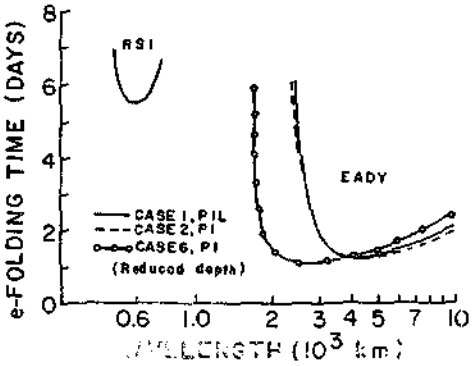

FIG. 3. Instability spectra of the cases 1, 2 and 6 (see Table 2). (Abscissa is zonal wavelength). RSI: Region of short scale instability. RII: Region of intermediate scale instability. EADY: Region of Eady mode instability.

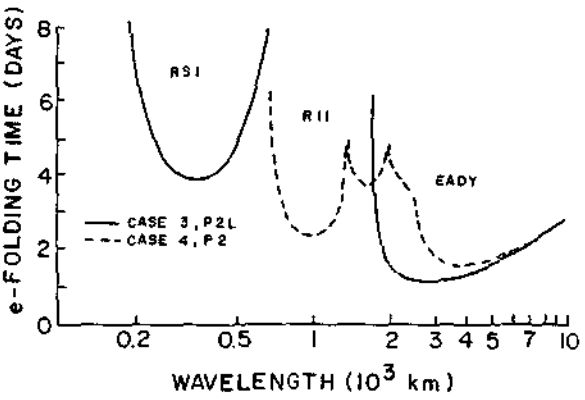

FIG. 4. As in Fig. 3 except for cases 3 and 4.

greater than $L_x = 2400$ km in case 1 (continuous curve) agrees well with the results obtained by Kuo (1953). It is well-known that, for constant shear profiles, there is a short wavelength cut-off with a most unstable wave (MUW) of wavenumber 8. The vertical structure of the MUW (not shown here) ($L_x = 4200$ km) looks exactly like the one obtained by Eady (1949) with the maximum amplitude of the geopotential at the horizontal rigid boundaries and symmetric with respect to the level $h/2$. This region of instability is referred to as Eady mode. In addition to the Eady mode, the profile P1L exhibits another region of short scale instability (RSI) with a MUW of 600 km. This RSI is obviously due to ageostrophic effects in the model, because test results without the inclusion of these ageostrophic effects did not produce RSI. The amplitude of the MUW of RSI is confined to the levels below 3 km. Kuo (1953), using a quasi-geostrophic model, obtained a similar vertical structure for subsynoptic-scale baroclinic waves, although he did not obtain two maxima in the growth rates. When the curvature of P1 is included (dashed curve in Fig. 3) the RSI disappeared while the Eady mode practically remained the same. This means that curvature of the type of P1 is not favorable for short-scale instability.

The IS of the profile P2L (case 3, continuous curve) and P2 (case 4, dashed curve) are shown in Fig. 4. The maximum value of S and the minimum value of Ri of P2L are about one fourth and one half, respectively, of those of P1L. This resulted in the RSI of P2L becoming more unstable than that of P1L. The Eady mode of P2L is shifted to shorter wavelengths, compared with that of P1L, because of the smaller value of static stability. This is a well-known characteristic of the Eady mode [see Houghton (1977) where the Eady wave solution for the zonal wavelength of the MUW is given by $L_m = 2\pi$ [illegible] is considered constant]. The short scale instability obtained in cases 1 and 3 does not agree with the numerical results obtained by Stone (1970).

The IS of P2 (dashed curve Fig. 4) presents sev-

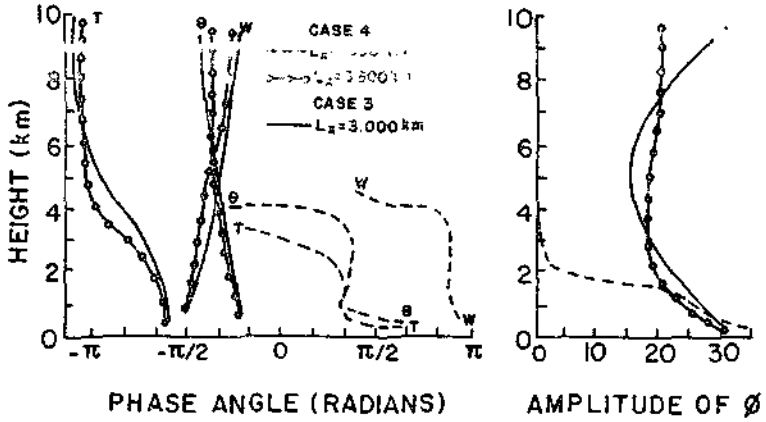

FIG. 5. Vertical structure of the unstable waves L_x = 1000 km and L_x = 3700 km in case 4 and L_x = 2400 km in case 3.

eral interesting characteristics. The Eady mode is not more stable and is shifted to longer wavelengths, because the maximum static stability of P2 is larger than the constant static stability of P2L. The RSI is stabilized, but an additional region of intermediate-scale instability (RII) with a MUW of L_x = 1000 km is generated. This shows that a low-level negative curvature of the basic zonal wind profile favors intermediate-scale instability. The e-folding time of the MUW in this RII is ~2.2 days and is comparable with that of the Eady mode (1.8 days). The structure of the Eady mode without the curvature effect (L_x = 2400 km in case 3), the Eady mode modified by the curvature effect (L_x = 3700 km in case 4) and the intermediate-scale wave (L_x = 1000 km in case 4) are shown in Fig. 5. The intermediate-scale wave is clearly seen to be confined to the lower levels.

For studying the effects of smaller static stability and smaller shear, the profile P3 is examined in case 5 and its IS is presented in Fig. 6 (continuous curve). The whole spectrum is displaced to shorter scales and e-folding times increase in comparison with case 4. The Eady mode presents a MUW of L_x = 1800 km in the intermediate scales and the RII is shifted to shorter scales with a MUW of 600 km. It seems that in a multilevel model, any small shear is sufficient to cause baroclinic instability if the static stability is sufficiently small, even if the Richardson number is considerably high. It is a known feature of the Eady mode that the wavelength of the MUW is proportional to the depth of the fluid (Houghton, 1977). This feature is verified in case 6 (curve with circles in Fig. 3) where the wavelength of the MUW is reduced to 2500 km (compare with case 2) with an e-folding time of roughly one day.

The studies of Blumen (1979) and Hyun (1981) showed the existence of the shorter-scale instability when one of the two layers was shallower than the other. The MUWs of the shorter scale instability in those studies were found at $\bar{k}(=kh\sqrt{S_a}/f) \approx 6$, where $\bar{k}$ is a nondimensional wavenumber. In case 4 of the present study the average static stability $S_a \approx 0.5 \times 10^{-4}$ s^{-2}, h = 10 km and $f \approx 0.73 \times 10^{-4}$ s^{-1}. So as to satisfy the above formula the wavelength of the MUW should be ~800 km, whereas the actual wavelength obtained in case 4 (see Fig. 4) is ~1000 km. Thus, our results agree qualitatively with those of Blumen and Hyun. The quantitative disagreement may be attributed to the model differences. The sharp jumps in S (Blumen, 1979) and $d\bar{u}/dz$ (Hyun, 1981) are rather unrealistic. In the present study these two parameters vary fairly smoothly. All the same we may note another qualitative agreement that the growth rate of the shorter scale MUW is smaller than that of the Eady mode. This has been the case even with an observed profile in the study of Mishra and Salvekar (1980).

A reduction of the static stability or the depth of fluid may bring the Eady mode to shorter scales, thereby presenting a MUW in the intermediate scales. However, a rather smooth variation of S and $d\bar{u}/dz$ in the vertical with a favorable curvature ($d^2\bar{u}/dz^2 < 0$) has generated a new region of subsynoptic-scale instability (case 4). These unstable waves are confined to lower levels.

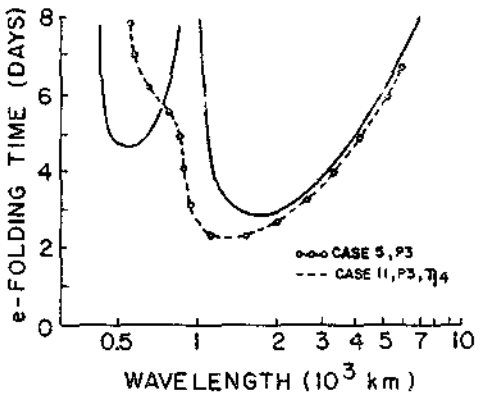

FIG. 6. As in Fig. 3 except for cases 5 and 11.

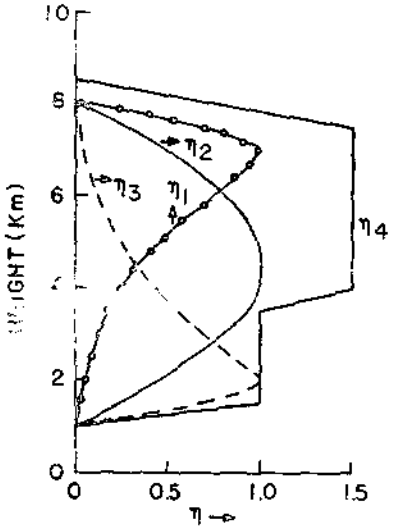

FIG. 7. Vertical profiles of the heating parameter.

b. Influence of wave-CISK

In the past many authors employed the heating due to liberation of latent heat to produce unstable modes at shorter scales (Nitta, 1964; Ooyama, 1969; Yamasaki, 1969). In this section a similar examination of the effects of wave-CISK mechanism on the IS is made. An important parameter included in our parameterization of wave-CISK is $\eta(z)$ (see Eq. 7). In a three-level model (equivalent to the conventional two-layer model) if $\eta < 1.0$, the wave-CISK alone cannot produce instability. To see this, consider $\bar{u} \equiv 0$ and η and S positive constants. In this case (5) is simplified to be

$$(f^2 - k^2c^2)\frac{d^2\tilde{w}}{dz^2} - k^2S\tilde{w} = -k^2S\eta\tilde{w}_* . \quad (13)$$

Applying this equation to the finite difference grid with $N = 3$ and $\tilde{w}_* = \tilde{w}_1$ we get the condition

$$\frac{f^2 - k^2c^2}{\Delta z^2} = \frac{1}{6}k^2S[(3\eta - 4) \pm (3\eta - 2)]. \quad (14)$$

From (14) we see that only with the plus sign can c become imaginary. In that case the necessary condition is $\eta > 1 + (f^2/k^2)S\Delta z^2$. Moreover, kc_i is maximum as $k \to \infty$ or $L_x \to 0$. In other words, the wave-CISK mechanism destabilizes very short scales.

A multilevel model, such as the present one, allows more realistic profiles of $\eta(z)$. The profiles used in the present study are shown in Fig. 7. The profiles η_1, η_2 and η_3 are generated by a function of the type $\eta \sim z^b \sin(z - z_c)/(z_t - z_c)$ where z_c and z_t are the cloud base and cloud top levels which are arbitrarily fixed to be 2 and 8 km, respectively. Such a function was used by [illegible]. For $b = 1, 0, -1$, the corresponding profiles have the peak values in the upper, middle or lower troposphere, respectively (see Fig. 7). The profile η_4 is an idealization of the one used by Shukla (1978) to study the monsoon disturbances whose scales are subsynoptic. The peak values of η used by Shukla are 2 and 3 whereas we use a peak value of 1.5 because the capacity of the midlatitude atmosphere to hold water vapor is smaller than that of the tropical atmosphere.

The height of the peak of the heating rate seems to have a profound effect on the baroclinic IS (Syono and Yamasaki, 1966). To examine this effect the IS of P1 with the inclusion of η_1, η_2 and η_3 are obtained in cases 7, 8 and 9, respectively. The basic state profile P1 is chosen because its curvature does not favor the subsynoptic-scale instability and any region of instability may safely be attributed to the diabatic heating alone. The results are shown in Fig. 8. The continuous and dashed curves show that the upper or middle tropospheric heating (with $\eta \leq 1$) does not produce new regions of appreciable instability. The curves with circles are due to the lower tropospheric heating (η_3). It shows, curiously, several regions of instability in the shorter and intermediate scales in addition to the Eady mode which has merged with the RII. The e-folding time of the MUW at L_x = 1800 km is almost equal to that of the Eady mode ($L_x \approx$ 4000 km). The complete structure of the MUW at L_x = 1800 km is shown in Fig. 9. It may be noted that the amplitudes are confined to the lower troposphere. Thus the lower-level heating is capable of generating intermediate-scale unstable waves whose characteristics resemble those of the observed intermediate-scale disturbances.

Gall (1976), in a study of the effects of release of latent heat on the unstable baroclinic waves, obtained a MUW around wavenumber 15 (zonal wavelength ~ 2500 km) both in dry and moist experiments with primitive equations. In his study the growth rate of the MUW is twice that of wavenumber 5 and the release of latent heat almost doubled its growth rate. In the present study the intermediate scale MUW has a wavelength of ~1800 km and its growth rate is not larger than that of a 4000 km wave. These discrepancies may be due to the lack of meridional

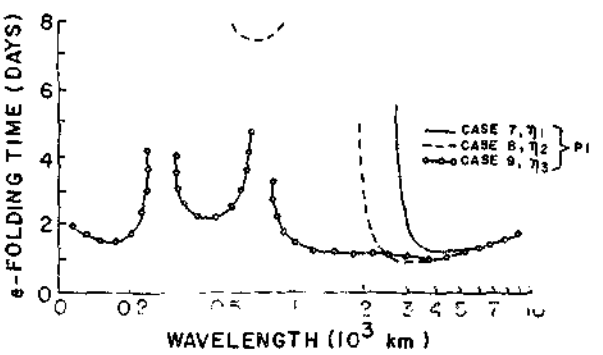

FIG. 8. As in Fig. 7 except for cases 7, 8 and 9.

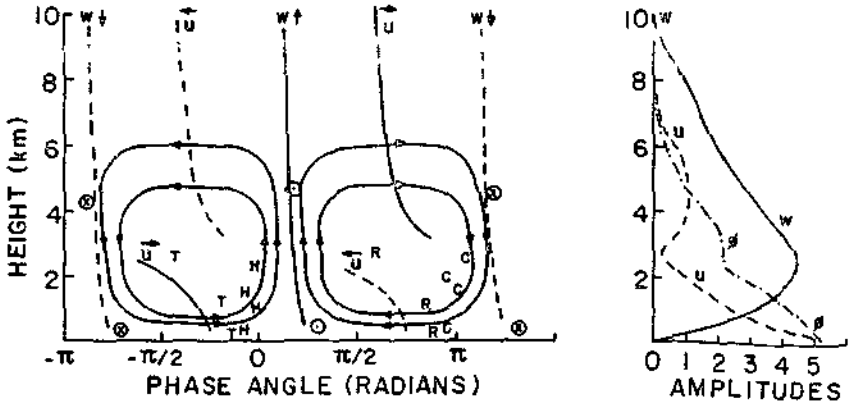

FIG. 9. Detailed structure of the unstable wave L = 1800 km in case 9. $\vec{u}$ = west wind maximum; $\overleftarrow{u}$ = east wind maximum; wl = downdraft maximum; wl = updraft maximum; T = trough; R = ridge; H = hot; C = cold; circle with cross = south wind; circle with dot = north wind. The solid lines with arrows are the streamlines.

variation and the differences in the parameterization of the release of latent heat in the present study. It may be noted, however, from Fig. 9 that the amplitudes of u and ϕ of the intermediate scale wave present a second peak around 5 km height which means that this wave has a second peak in Kinetic energy at that height. This is in good agreement with the results of Gall (see Fig. 11 in Gall, 1976).

Case 10 is obtained by introducing η_4 in case 4. The diabatic heating slightly reduced the scale and e-folding time of the Eady mode. Surprisingly, it increases the scale of the MUW of RII to 1600 km (continuous curve in Fig. 10). Case 11 is obtained by including η_4 in case 5 and the resulting IS is shown by the curve with circles in Fig. 6. We may note that the heating merged the two regions of instability with a single MUW at L_x = 1200 km. The structure of this wave, given in Fig. 11, shows that its amplitude is maximum in the lower troposphere, although it does not fall off sharply with height.

From these results we may conclude that the diabatic heating slightly increases the growth rates and decreases the scale of the Eady mode, and low-level heating is favorable for the subsynoptic-scale instability.

c. *Effects of β and l*

The well-known effect of β is to stabilize very long waves. The Eady mode modified by the β-effect is referred to as the Eady-Charney mode. The effect of the meridional variation of the perturbations ($l \neq 0$) is to decrease the growth rates and increase the scale of the Eady-Charney mode. It is known that for a given k (or L_x) the growth rate of the Eady-Charney mode is maximum for l = 0 (Green, 1960). For a qualitative discussion, in the case where l is different from zero, it is put equal to k, i.e., $l = k$. In this case the wave moves at a 45° angle to the basic flow.

Cases 12 and 13 are obtained by including β in cases 1 and 2, respectively, and case 14 is obtained by including η_4 in case 13. The IS for these three cases are shown in Fig. 12. All three IS have long-wavelength cutoffs. It appears that β slightly increases the instability of the subsynoptic modes (compare with Fig. 3). It can be seen that the RSI is stabilized by the effect of the curvature of PI and the diabatic heating again increased the instability of this region as is the case in f-plane model.

Case 15 is obtained by introducing $l = k$ in case 13. The IS is presented in Fig. 12 (curve with crosses). In case 15 the horizontal wavelength is given by $L_x/\sqrt{2}$, because $l = k$ in the expression $L = 2\pi(1/k^2 + 1/l^2)^{1/2}$. Thus the wavelengths of the MUWs of the Eady mode in the two cases 13 and 15 agree well. This IS shows that the e-folding time of the Eady-Charney mode is increased in comparison with case 13. In addition, the meridional variation produced a new region of instability at wavelengths less than 100 km. The maximum instability is tending to occur in the shortest scales. These modes are, apparently, not due to Kelvin-Helmholtz insta-

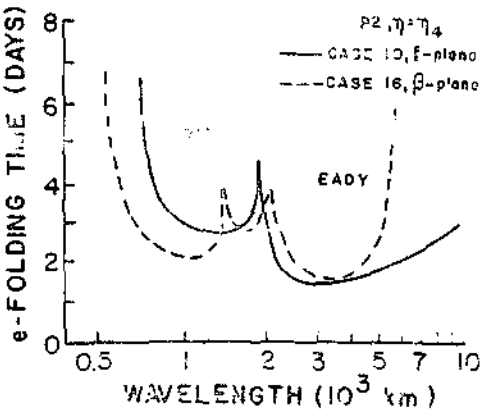

FIG. 10. As in Fig. 3 except for cases 10 and 16.

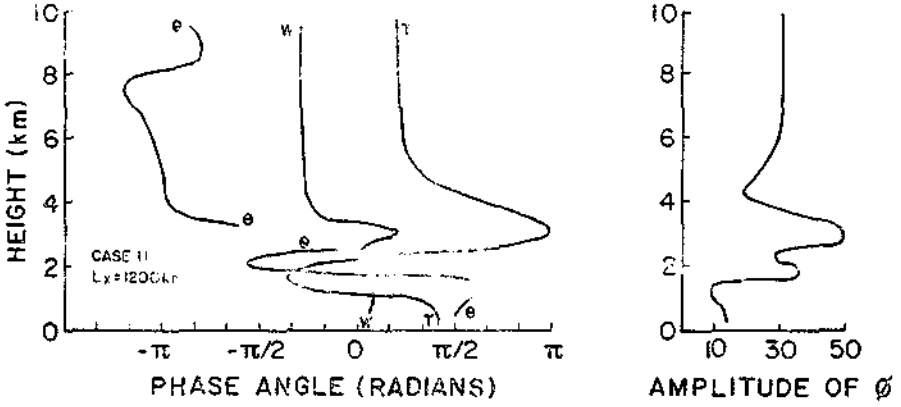

FIG. 11. As in Fig. 5 except for L_x = 1200 km in case 11.

bility because Stone's (1966) results show that this kind of instability appears only for Ri < 0.25 whereas in the present case Ri > 1.0. For very small-scale waves the non-hydrostatic or non-Boussinesq effects become important and the results obtained in the present study do not represent their behavior.

Case 16 is obtained by including β in case 10 and the IS is presented in Fig. 10 (dashed curve). The results show clearly that the effect of the curvature of P2 type (favorable for intermediate-scale instability) remains the same even in the β-plane model. The growth rates of the RII increased slightly while those of the Eady-Charney mode decreased slightly. The structure of the MUW of the RII in this case remained the same as in case 10 (not shown here).

In Fig. 13 the energetics of the intermediate-scale wave are compared with those of Eady-Charney mode of case 10. The energy conversion from $\bar{K}$ to K' is due to the term $(d\bar{u}/dz)\overline{u'w'}$ alone because there is no meridional variation of the basic states. It may be noted that the shorter-scale mode converts its potential energy into kinetic energy almost at the same rate as it receives it from the basic state, whereas the Eady-Charney mode retains a substantial part in its potential energy. That is, the kinetic energy of the intermediate-scale unstable wave grows faster than its potential energy.

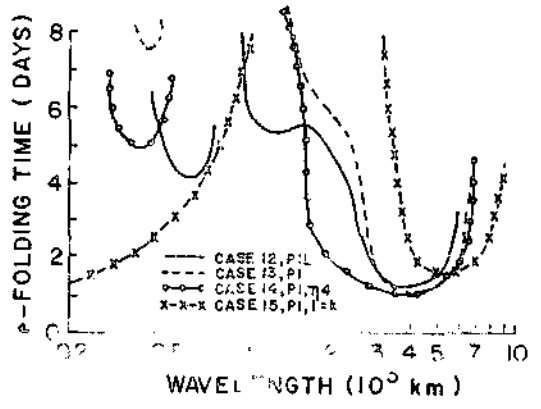

FIG. 12. As in Fig. 11 for cases 12, 13, 14 and 15.

4. Conclusions

The results presented in the preceding section show that the curvature $(d^2\bar{u}/dz^2)$ of the basic zonal wind profile is important for the instability of the subsynoptic-scale perturbations. It seems that a negative curvature in the lower levels favors destabilization of a new region in the intermediate scales (L_x ~ 1000 km) of the spectrum while a positive curvature stabilizes the subsynoptic waves. The intermediate-scale unstable waves have their amplitudes confined to the lower troposphere. Low-level heating due to the liberation of latent heat is also capable of generating instability in the subsynoptic scales besides increasing the growth rates of the pre-existing modes. Reduction of static stability and shear (Richardson number not necessarily small) reduces the scale of the Eady mode to produce intermediate-scale instability. In the real atmosphere this may not be the case because the important parameters in determining the preferred scale of the Eady mode seem to be the depth of the fluid and the average static stability. The intermediate and shorter-scale unstable modes obtained in the dry cases agree qualitatively with those obtained by Blumen (1979) and Hyun (1981). The vertical structure of the intermediate-scale fastest growing wave, in the case with

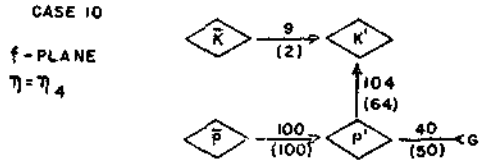

FIG. 13. Energy conversion in case 10. Numbers without parentheses: L_x = 3000 km; numbers in parentheses: L_x = 1000 km; $\bar{P}$ = potential energy of the basic state; $\bar{K}$ = kinetic energy of the basic state; P' = potential energy of the perturbation; K' = kinetic energy of the perturbation; G = generation.

[illegible] in the lower levels, [illegible] double peaked kinetic energy structure [illegible] by Gall (1976).

The Green's modes obtained in the β-plane model beyond L_x = 8000 km had e-folding times greater than eight days and they were not presented in the results. There are some limitations in the present study. The meridional variation of the basic state is not considered and a rigid lid is assumed at the top. The first limitation renders the results inapplicable to a front. It can be overcome if larger computational facility is made available, although a new difficulty about fixing the appropriate lateral boundary conditions is likely to appear. The rigid top may be removed by imposing a radiation condition at the upper boundary. However, the rigid top may not affect the short- or intermediate-scale waves which are found to be bottom trapped, as long as it is placed high enough, as is done in the present study.

Acknowledgments. The suggestions of Prof. P. H. Stone (MIT) during the initial stages of the work have been useful. We thank Drs. P. Tissi (INPE) and Eugenia Kalnay (GLAS/NASA) for the discussions on the numerical problem and Dr. Dean Duffy (GLAS/NASA) for critically reviewing the manuscript. The continued encouragement and support extended by Drs. N. J. Parada and L. G. Meira Filho of the Instituto de Pesquisas Espaciais (INPE) are gratefully acknowledged. The reviewers' suggestions and comments have been very helpful. Thanks are due to Mrs. Tânia Regina Freire Sanchez for typing the manuscript. This work is taken from the first author's thesis and is partially supported by Convênio FINEP/CNPq B/28/79/002 Modelagem Atmosférica.

REFERENCES

Blumen, W., 1979: On short-wave baroclinic instability. *J. Atmos. Sci.*, **36**, 1925–1933.

Carleton, A. M., 1979: A synoptic climatology of satellite observed extratropical cyclone activity for the Southern Hemisphere winter. *Arch. Meteor. Geophys. Bioklim.*, **27**, 265–279.

Chang, C. P., 1976: Vertical structure of tropical waves maintained by internally-induced cumulus heating. *J. Atmos. Sci.*, **33**, 729–739.

Charney, J. G., 1947: The dynamics of long waves in a baroclinic westerley current. *J. Meteor.*, **4**, 135–162.

——, 1973: Planetary fluid dynamics. *Dynamic Meteorology*, D. Reidel, 97–351.

——, 1975: Jacob Bjerknes—An appreciation. *Selected Papers of Bjerknes*, University of California, Los Angeles, 11–13.

Duffy, D. G., 1978: The stability of a nonlinear, finite amplitude, neutrally stable Eady wave. *J. Atmos. Sci.*, **35**, 1619–1625.

Eady, E. T., 1949: Long waves and cyclone waves. *Tellus*, **1**, 33–52.

[illegible] On the initial development of [illegible] *Meteor. Inst.*, No. 13, 107 pp.

Gall, R., 1976: The effects of released latent heat in growing baroclinic waves. *J. Atmos. Sci.*, **33**, 1686–1701.

Garbow, B. S., 1978: The QZ algorithm to solve the generalized eigenvalue problem for complex matrices (F2). *ACM Trans. Math. Software*, **4**, 404–410.

Green, J. S. A., 1960: A problem in baroclinic stability. *Quart. J. Roy. Meteor. Soc.*, **86**, 237–251.

Houghton, J. T., 1977: *The Physics of Atmospheres*. Cambridge Univ. Press, 203 pp.

Hyun, J. M., 1981: Separate and combined effects of static stability and shear variation on the baroclinic instability of a two-layer current. *J. Atmos. Sci.*, **38**, 322–333.

Kuo, H-L, 1952: Three-dimensional disturbances in a baroclinic zonal current. *J. Meteor.*, 260–278.

——, 1953: The stability properties and structure of disturbances in a baroclinic atmosphere. *J. Meteor.*, **10**, 235–243.

Matsumoto, S., S. Yoshizumi and M. Takeuchi, 1970: On the structure of the "Baiu-front" and the associated intermediate-scale disturbances in the low atmosphere. *J. Meteor. Soc. Japan*, **48**, 479–491.

Mishra, S. K., and P. S. Salvekar, 1980: Role of baroclinic instability in the development of monsoon disturbances. *J. Atmos. Sci.*, **37**, 383–394.

Mullen, S. L., 1979: An investigation of small synoptic-scale cyclones in polar air streams. *Mon. Wea. Rev.*, **107**, 1636–1647.

Nitta, T., 1964: On the development of the relatively small-scale cyclone due to the release of latent heat of condensation. *J. Meteor. Soc. Japan*, **42**, 260–276.

——, and Y. Ogura, 1972: Numerical simulation of the development of the intermediate-scale cyclone in a moist atmosphere. *J. Atmos. Sci.*, **29**, 1011–1024.

Ooyama, K., 1969: Numerical simulation of the life cycle of tropical cyclones. *J. Atmos. Sci.*, **26**, 3–40.

Orlanski, I., 1968: Instability of frontal waves. *J. Atmos. Sci.*, **25**, 178–200.

Phillips, N. A., 1954: Energy transformation and meridional circulations associated with simple baroclinic waves in a two-level quasi-geostrophic model. *Tellus*, **6**, 273–286.

——, 1970: Models for weather prediction. *Annual Review of Fluid Mechanics*, Vol. 2, Annual Reviews, Inc., 251–292.

Rasmussen, E., 1979: The polar low as an extratropical CISK mechanism. *Quart. J. Roy. Meteor. Soc.*, **105**, 531–549.

Reed, R. J., 1979: Cyclogenesis in polar air streams. *Mon. Wea. Rev.*, **107**, 38–52.

Shukla, J., 1978: CISK—barotropic baroclinic instability and the growth of monsoon depressions. *J. Atmos. Sci.*, **35**, 495–508.

Solberg, H., 1928: Intergrationer der atmospharischen Storungsgleichungen. *Geofys. Publ.*, **5**, 120 pp.

Staley, D. O., and R. L. Gall, 1977: On the wavelength of maximum baroclinic instability. *J. Atmos. Sci.*, **34**, 1679–1688.

Stone, P. H., 1966: On non-geostrophic baroclinic stability. *J. Atmos Sci.*, **23**, 390–400.

——, 1970: On non-geostrophic baroclinic stability: Part II. *J. Atmos. Sci.*, **27**, 721–726.

Syono, S., and M. Yamasaki, 1966: Stability of symmetrical motions driven by latent heat released by cumulus convection under the existence of surface friction. *J. Meteor. Soc. Japan*, **44**, 353–375.

Yamasaki, M., 1969: Large-scale disturbances in the conditionally unstable atmosphere in low latitudes. *Pap. Meteor. Geophys.*, **20**, 289–336.